ORIGINAL ARTICLE



A self-triggered radioligand therapy agent for fluorescence imaging of the treatment response in prostate cancer

Hongchuang Xu¹ · Yanpu Wang² · Jingming Zhang¹ · Xiaojiang Duan¹ · Ting Zhang² · Xuekang Cai¹ · Hyunsoo Ha³ · Youngjoo Byun³ · Yan Fan¹ · Zhi Yang^{4,5} · Yiguang Wang⁶ · Zhaofei Liu^{2,5} · Xing Yang^{1,5,7}

Received: 24 November 2021 / Accepted: 20 February 2022 / Published online: 2 March 2022 © The Author(s), under exclusive licence to Springer-Verlag GmbH Germany, part of Springer Nature 2022

Abstract

Purpose Radioligand therapy (RLT) targeting prostate-specific membrane antigen (PSMA) is emerging as an effective treatment option for metastatic castration-resistant prostate cancer (mCRPC). An imaging-based method to quantify early treatment responses can help to understand and optimize RLT.

Methods We developed a self-triggered probe **2** targeting the colocalization of PSMA and caspase-3 for fluorescence imaging of RLT-induced apoptosis.

Results The probe binds to PSMA potently with a K_i of 4.12 nM, and its fluorescence can be effectively switched on by caspase-3 with a K_m of 67.62 μ M. Cellular and in vivo studies demonstrated its specificity for imaging radiation-induced caspase-3 upregulation in prostate cancer. To identify the detection limit of our method, we showed that probe 2 could achieve 1.79 times fluorescence enhancement in response to 177 Lu-RLT in a medium PSMA-expressing 22Rv1 xenograft model. Conclusion Probe 2 can potently bind to PSMA, and the fluorescence signal can be sensitively switched on by caspase-3 both in vitro and in vivo. This method may provide an effective tool to investigate and optimize PSMA-RLT.

 $\textbf{Keywords} \ \ Radioligand \ the rapy \cdot Prostate \ cancer \cdot Prostate-specific \ membrane \ antigen \ (PSMA) \cdot Self-triggered \ probe \cdot Caspase-3$

Hongchuang Xu and Yanpu Wang contributed equally to this work.

This article is part of the Topical Collection on Theragnostic.

- ☑ Zhaofei Liu liuzf@bjmu.edu.cn
- Xing Yang yangxing 2017@bjmu.edu.cn

Hongchuang Xu xhc@bjmu.edu.cn

Yanpu Wang wangyp@bjmu.edu.cn

- Department of Nuclear Medicine, Peking University First Hospital, Beijing 100034, China
- Medical Isotopes Research Center and Department of Radiation Medicine, School of Basic Medical Sciences, Peking University Health Science Center, Beijing 100191, China

Introduction

Prostate cancer is the second most commonly diagnosed malignancy in men worldwide [1]. Effective treatments have been developed to manage prostate cancer at different stages [2]. Among the various therapies, radiation therapy

- College of Pharmacy, Korea University, 2511 Sejong-ro, Sejong 30019, South Korea
- ⁴ Key Laboratory of Carcinogenesis and Translational Research (Ministry of Education/Beijing), Department of Nuclear Medicine, Peking University Cancer Hospital & Institute, Beijing 100142, China
- ⁵ NMPA Key Laboratory for Research and Evaluation of Radiopharmaceuticals, Beijing 100142, China
- State Key Laboratory of Natural and Biomimetic Drugs, Peking University, Beijing 100191, China
- Institute of Medical Technology, Peking University Health Science Center, Beijing 100191, China



plays an important role. External beam radiotherapy (EBRT) or low-dose brachytherapy has become a routine option for patients with high-risk nonmetastatic prostate cancer [3]. Toward a cure for lethal mCRPC, RLT targeting PSMA, a cell surface protein overexpressed specifically in prostate cancer, has emerged as a state-of-the-art technique and showed improved therapeutic efficacy and safety in multiple clinical trials [4–6]. Different from conventional external radiation therapy focusing on localized lesions, RLT is based on the highly specific delivery of therapeutic radioisotopes, such as the β -emitter ¹⁷⁷Lu or the α -emitter ²²⁵Ac, targeting cancer-specific biomarkers expressed on metastatic lesions [7, 8]. Although PSMA expression is normally confirmed by PSMA-positron emission tomography/computed tomography (PET/CT) before PSMA-RLT, there are still patients with mCRPC who show poor responses [4]. There are currently several methods to determine treatment response, including serum PSA level measurement, computed tomography (CT), and PSMA-PET/CT [9, 10], but all these examinations are based on a reduced tumor burden, which normally takes weeks to months to show a significant change. A method that could detect the early response to RLT before the tumor starts to shrink would provide timely feedback information to help adjust therapy for patients.

Ionizing radiation can induce the generation of reactive oxygen species and trigger either organic reactions or downstream cellular responses. It can be used to design radiation-activatable fluorescence sensors or prodrugs, and recently, its feasibility has been demonstrated in X-ray-based radiotherapy (RT) [11–13]. Compared with external RT, the radiation dose of RLT is mainly limited by the receptor density, and the therapeutic efficacy of PSMA-RLT may also vary due to the heterogeneous expression of PSMA in or among patients [14]. PSMA-RLT requires higher sensitivity to detect the cellular response of small lesions with low PSMA expression, and the feasibility has not yet been proven. Enzyme-activated fluorescence sensors could potentially improve the sensitivity due to their inherent catalytic signal-enhancing mechanism [15]. Caspase-3, a key enzyme mediating apoptosis [16], is upregulated rapidly in response to radiation treatment [17], and it is an ideal biomarker for monitoring the early stages of apoptosis [18]. It can catalyze the hydrolysis of the peptide sequence DEVD at the N-terminus, enabling the design of sensors with high sensitivity and specificity [17, 19, 20]. We hypothesized that a probe specifically targeting the colocalization of PSMA and caspase-3 with a fluorescence switch activated by caspase-3 upregulation would provide enough sensitivity to image the early treatment response of RLT.

Hemicyanine dyes, owing to their near-infrared (NIR) emission, strong excited-state intramolecular charge transfer (ICT), and high quantum yield, are highly suitable for in vivo imaging. Hemicyanine-based NIR activatable probes

(HNAPs) can be effectively designed by caging electron donors (NH₂ or OH groups) on aromatic scaffolds with biomarker-responsive moieties, and tens of fold fluorescence enhancement can be achieved upon activation, which has recently attracted worldwide attention for the design of high-sensitivity fluorescence sensors, including reactive oxygen species, nitrogen species, sulfur species, and enzymes [21–24]. In this study, we designed a PSMA-targeting ¹⁷⁷Lu-RLT agent embedded with a self-triggered HNAP and demonstrated the feasibility of specifically imaging the early treatment response of RLT in a medium PSMA-expressing tumor xenograft model.

Material and methods

Chemical synthesis

Probe **2** was synthesized using solid-phase synthesis and purified by high-performance liquid chromatography (HPLC) to reach > 95% purity. The procedures and characterization are described in the Supplementary Information.

The UV-Vis and fluorescence spectra of probes

Ultraviolet–visible (UV–Vis) and fluorescence spectra were collected using a UV–Vis spectrophotometer (UH5300, Hitachi, Japan) and a fluorescence spectrometer (F-7000, Hitachi, Japan), respectively. A total of 5 μ M 1 or 2 was dissolved in assay buffer containing 50 mM HEPES, 50 mM NaCl, 10 mM EDTA, 10 mM DTT, and 5% glycerol. UV–Vis spectra were acquired from 500 to 750 nm. The fluorescence spectra were obtained at an excitation wavelength of 670 nm, and the emission spectra were scanned in the range of 650 to 850 nm.

To determine caspase-3-triggered fluorescence enhancement, $10~\mu M~2$ was incubated with or without 2.5 U/ml recombinant human caspase-3 (BioVision, CA, USA, Catalog no. 1083-100) at 37 °C for 48 h. Fluorescence spectra were collected with the settings mentioned above.

Time-dependent fluorescence activation mediated by caspase-3

Probe **2** (50 μ M) was mixed with 2.5 U/ml recombinant human caspase-3 in assay buffer in a 96-well plate (Corning, NY, USA) to a final volume of 200 μ L. The no enzyme or 1 mM caspase-3 inhibitor group was used as the control. After mixing, the plate was placed into a microplate reader (BioTek, Winooski, VT, USA). The fluorescence intensity was monitored hourly at 37 °C for 6 h ($\lambda_{EX}/\lambda_{EM}=670/700$ nm). The data were linearly fitted using



GraphPad Prism software (San Diego, CA, USA). Each experiment was performed in triplicate.

Caspase-3 concentration-dependent fluorescence activation

Probe **2** (50 μ M) was mixed with different concentrations of recombinant human caspase-3 in the assay buffer in a 96-well plate to a final volume of 200 μ L, including 0.125 U/ml, 0.25 U/ml, 0.5 U/ml, 3 U/ml, and 6 U/ml. After mixing, the plate was placed into a microplate reader. The fluorescence intensity of the mixture was measured at 37 °C ($\lambda_{EX}/\lambda_{EM}$ = 670/700 nm) at 1 h. The initial intensity at 0 h was also recorded as the baseline, and the fluorescence intensity increase was calculated. The data were fitted using a linear regression equation calculated in GraphPad Prism software. Each experiment was performed in triplicate.

Enzyme kinetics measurement

Caspase-3 protein (2.5 U/ml) was incubated with different concentrations of **2** in assay buffer at 37 °C, including 5 μ M, 10 μ M, 50 μ M, 100 μ M, 200 μ M, and 400 μ M. The fluorescence intensity of the mixture was measured at 6 h using a microplate reader ($\lambda_{\rm EX}/\lambda_{\rm EM}=670/700$ nm). The initial intensity at 0 h was also recorded as the baseline, and the fluorescence intensity increase was calculated. The data were fitted using a nonlinear regression equation, and $K_{\rm m}$ was calculated in GraphPad Prism using the Michaelis–Menten equation. Each experiment was performed in triplicate.

In silico docking study

- (1) Ligand preparation and optimization: Probe **2** was generated as a 3D structure by Chem3D Pro (ver 20.0.0.41, PerkinElmer, Waltham, MA, USA). Ligand optimization was performed by the Sanitize preparation protocol in SYBYL-X (ver 2.1.1., Tripos Inc., St. Louis, MO, USA).
- (2) Protein preparation: The PSMA structure was obtained from the RCSB Protein Data Bank (PDB ID: 505R). The crystal ligand and water molecules of the crystal structure were removed. Hydrogen atoms were added under the application of the Amber7 FF99 Force Field setting. The minimization process was performed by the Powell method. The initial optimization option was set to none.
- (3) Docking study: The docking study of the prepared probe **2** was performed by the Surflex-Dock GeomX module of SYBYL-X. The Surflex-Dock protomol site was generated by using the residue method. Selected amino acids: Arg181, Thr182, Glu183, Lys207, Phe209, Arg210, Lys213, Asn257, Ser318, Glu424, Leu428,

Arg463, Lys499, Pro504, Arg511, Lys514, Ser517, Gly518, Asn519, Arg534, Arg536, Trp541, Glu542, Thr543, Asn544, Lys545, Phe546, Ser547, Gly548, Lue551, Tyr552, His553, Lys606, Lys610, Ile614, Met616, His697, Lys699, Try700, Glu703, Tyr709, and Phe713; radius setting: 5.0; threshold: 0.60. Other parameters were applied with its default settings.

Cell lines and mouse models

LNCaP, 22Rv1, and PC3 human prostate cancer cell lines were purchased from the Chinese Academy of Sciences Typical Culture Collection (Shanghai, China) and cultured at 37 °C in a humidified atmosphere containing 5% CO₂. LNCaP cells were cultured with RPMI 1640 medium plus 10% fetal bovine serum (FBS), 1% penicillin-streptomycin, 1% GlutaMAX-I, and 1% sodium pyruvate. 22Rv1 and PC3 cells were cultured in RPMI 1640 medium plus 10% fetal bovine serum (FBS) and 1% penicillin-streptomycin. All animal studies were carried out in conformity to regulations on laboratory animals of the Beijing municipality and approved by the Animal Ethics Committee at Peking University Frist Hospital (Beijing, China), approval number J202163. All mice were obtained from the Animal Center at the Peking University First Hospital and acclimatized for at least 7 days before further experiments. Four-week-old male BALB/c nude mice were inoculated subcutaneously with 22Rv1 or PC3 (10⁷ cells/mouse) cells in the left flank. Mice were used for imaging when the xenografts reached $300-500 \text{ mm}^3$.

In vitro cytotoxicity

LNCaP, 22Rv1, and PC3 cells were seeded in 96-well culture plates (5000 cells per well) and incubated for 24 h. The cells were then treated with medium containing different concentrations of probe 2 for 48 h, including 5 μM , 10 μM , 25 μM , 50 μM , 100 μM , and 200 μM . Cell viability was determined by the thiazolyl blue tetrazolium bromide (MTT) assay using a microplate reader. The viability of the untreated controls was normalized to 100%, and the medium absorbance was set as the background. Each experiment was performed in triplicate.

Cell uptake studies

To determine the cellular uptake of 177 Lu-labeled **2**, 10^5 LNCaP, 22Rv1, or PC3 cells were seeded in poly-L-lysine-coated 24-well cell culture plates and incubated for 48 h. The cells were incubated with 50 μ L of RPMI 1640 medium containing 22.5–30 kBq of 177 Lu-labeled **2**. The specificity of the uptake was determined by blocking the cells with 100 μ M PSMA inhibitor ZJ43. All experiments were



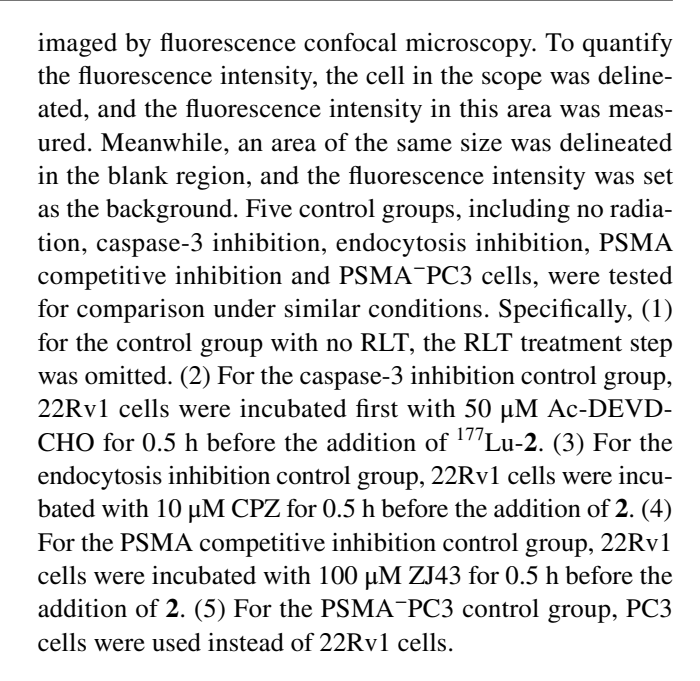
conducted at 37 °C, and the incubation was terminated at 1 h by washing 3 times with 1 mL of ice-cold phosphate-buffered saline. The cells were lysed with 0.5 M NaOH, and the radioactivity was measured in a gamma counter (Packard, Meriden, CT). To determine the internalization rate, a washing step (glycine–HCl, 50 mM, pH 2.8) was performed before lysing the cells. The uptake was calculated as the percent of the initially added radioactivity bound to 10⁵ cells. The internalization rate was calculated as a percentage value of uptake. All experiments were conducted in triplicate.

Imaging of living cells responding to RT

22Rv1 or PC3 cells were seeded in a 96-well culture plate at 5000 cells per well and incubated for 24 h. The experiments were divided into six groups, including the PSMA⁺ 22Rv1treated group and five control groups. For the treatment group, 22Rv1 cells were irradiated with 8 Gy by an X-ray irradiator (Rad Source Technologies, GA), and after 48 h, the cells were incubated with 100 µM 2 for another 12 h at 37 °C. Then, the cells were treated with Hoechst 33,342 (Solarbio, Beijing, China; 1:1000 dilution) for 10 min and subsequently imaged by confocal microscopy (Leica, TCS-SP8 STED 3X, Germany). To quantify the fluorescence intensity, the cell in the scope was delineated, and the fluorescence intensity in the area was measured. Meanwhile, an area of the same size was delineated in the blank region, and the fluorescence intensity was set as background. Five control groups, including no radiation, caspase-3 inhibition, endocytosis inhibition, PSMA competitive inhibition, and PSMA⁻ PC3 cells, were tested under similar conditions for comparison. Specifically, (1) for the control group with no radiation, the X-ray irradiation step was omitted; (2) for the caspase-3 inhibition group, 22Rv1 cells were incubated with 50 μM Ac-DEVD-CHO for 0.5 h before the X-ray irradiation step; (3) for the endocytosis inhibition group, 22Rv1 cells were incubated with 10 µM chlorpromazine (CPZ) for 0.5 h before the addition of 2; 4) For the PSMA competitive inhibition control group, 22Rv1 cells were incubated with 100 μM ZJ-43 for 0.5 h before the addition of 2; 5) For the PSMA⁻ PC3 control group, PC3 cells were used instead of 22Rv1 cells.

Imaging of living cells responding to RLT

22Rv1 or PC3 cells were seeded in a 96-well culture plate at 5000 cells per well and incubated for 24 h. The experiments were divided into six groups, including the PSMA⁺ 22Rv1-treated group and five control groups. In the treated group, 22Rv1 cells were treated with 370 kBq ¹⁷⁷Lu-**2**, and after 48 h, the cells were incubated with 100 μM **2** for another 12 h at 37 °C. Then, the cells were incubated with Hoechst 33342 (1:1000 dilution) for 10 min and subsequently



In vivo imaging of prostate tumors responding to RT

PSMA⁺ 22Rv1 or PSMA⁻ PC3 xenografts were randomly divided into one treated group and three control groups (n=5) for radiation treatment groups and n=4 for no radiation groups). For the treated group, 22Rv1 tumor-bearing mice were irradiated with 8 Gy by an X-ray irradiator. After 48 h, 22Rv1 tumor-bearing mice were administered 200 nmol 2 in 100 µL PBS buffer, and then the images were acquired at 1 h, 4 h, 12 h, 24 h, 48 h, and 72 h by the IVIS optical imaging system (Xenogen, Alameda, CA), using autoexposure with E_x/E_m set to 670/710 nm. To quantify the results, the tumor area was delineated with bright field. The animals were sacrificed at 72 h after imaging. Organs of interest were dissected, blotted, and weighed. The fluorescence signals of organs were measured by an IVIS optical imaging system. Three control groups, including no RT, PSMA-PC3 tumors with RT, and PSMA-PC3 tumors without RT, were tested for comparison under similar conditions. Specifically, (1) for the no RT control group, the RT treatment step was omitted; (2) for the PSMA-PC3 tumor with RT control group, PC3 tumor-bearing mice were used instead of 22Rv1; (3) for the PSMA-PC3 tumor without RT control group, PC3 tumor-bearing mice were used instead of 22Rv1, and the RT treatment step was omitted.

In vivo imaging of prostate tumors responding to RLT

Mice bearing PSMA⁺ 22Rv1 or PSMA⁻ PC3 xenografts were randomly divided into one treatment group and three control groups (n=4). For the treatment group, 22Rv1 tumor-bearing mice were treated with 18.5 MBq 177 Lu-2.



After 48 h, 22Rv1 tumor-bearing mice were administered 200 nmol 2 in 100 µL PBS buffer, and then the images were acquired at 1 h, 4 h, 12 h, 24 h, 48 h, and 72 h by the IVIS optical imaging system, using autoexposure with the E_x/E_m set to 670/710 nm. To quantify the images, the tumor area was delineated with bright field. The animals were sacrificed at 72 h after imaging. Organs of interest were dissected, blotted, and weighed. The fluorescence signals of organs were measured by an IVIS optical imaging system. Three control groups, including no RLT, PSMA-PC3 tumors with RLT, and PSMA⁻PC3 tumors without RLT, were tested for comparison under similar conditions. Specifically, (1) for the no RLT control group, the RLT treatment step was omitted; (2) for the PSMA⁻PC3 tumor with RLT control group, PC3 tumor-bearing mice were used instead of 22Rv1; (3) for the PSMA⁻PC3 tumor without RLT control group, PC3 tumor-bearing mice were used instead of 22Rv1, and the RLT treatment step was omitted.

Immunofluorescence staining

Frozen slices of 22Rv1 and PC3 tumor tissues were fixed with ice-cold acetone, rinsed with PBS, and blocked with 10% bovine serum albumin for 30 min at room temperature. The slices were incubated with anti-cleaved caspase-3 anti-bodies (Abcam, Cambridge, UK; 1:100 dilution) for 12 h at 4 °C and then visualized with DyLight 549-conjugated secondary antibodies (EarthOx, Millbrae, CA; 1:200 dilution) under a Leica TCS-NT confocal microscope (Wetzler, Heidelberg, Germany).

Statistical analysis

All data are presented as the mean values \pm S.D. Significant differences in quantitative data were analyzed by conducting Student's *t*-test or one-way analysis of variance (ANOVA) Tukey's multiple comparisons test depending on the number of treatment groups and distribution. Statistical significance was considered at a P < 0.05.

Results

Design and synthesis of a radiation-triggered probe targeting prostate cancer

To monitor caspase-3 levels in prostate cancer during RLT treatment, we designed a radiation-triggered probe containing a caspase-3 activatable fluorescent sensor, a PSMA targeting group, and a metal chelating group for labeling the radioisotope ¹⁷⁷Lu (Fig. 1a and b). N-acylated hemicyanine dye 1 was chosen as the caspase-3 activatable fluorescent sensor. We hypothesized that caspase-3 could specifically

hydrolyze DEVD-1 and release the electron-donating NH₂ group in 1, resulting in an enhancement of fluorescence intensity at the NIR region through ICT [19, 25-27]. A series of low-molecular-weight agents have been reported for PSMA targeting with both high potency and selectivity, including Glu-Ureas [28], Glu-Carbamates [29], ODAP-Ureas [30], and so on. Glu-Urea-Glu was selected as the PSMA targeting moiety to facilitate synthesis. ¹⁷⁷Lu, as a β-emitter with a half-life of 6.65 days, is an ideal radioisotope for RLT [31] and was chosen for our study. It can be efficiently and stably labeled by the metal chelator 1,4,7,10-tetraazacyclododecane-1,4,7,10-tetraacetic acid (DOTA) [32]. Compared with α -emitters, the low-energy irradiation by the β -emitter could help us test the detection limit of the method. After optimization, the designed probe 2 could be assembled with reasonable yield (14%) using tenstep solid-phase synthesis (Figs. 1b and S1). The final product was purified by HPLC to reach > 95% purity and characterized by high-resolution mass spectrometry (Fig. S2).

Biochemical and biophysical characterization of the probe

The optical property was tested first. Free dye 1 displayed an absorbance peak at 670 nm, while that of 2 with caged NH₂ was blueshifted to 606 nm, and the fluorescence emission peaked at 710 nm for 1 and 690 nm for 2 (Figs. 1c and S3). Dye 1 exhibited a 10.6-fold higher fluorescence intensity than 2 at 710 nm. Upon incubation with caspase-3, 2 could be activated, resulting in a time-dependent fluorescence intensity increase (Fig. 1d). This fluorescence enhancement could be significantly inhibited by a known caspase-3 inhibitor, Ac-DEVD-CHO [33], indicating its specificity. A linear correlation was also observed between caspase-3 concentration and the fluorescence increase (Fig. 1e). Within 1 h, 0.125 U/ml caspase-3 could be detected. The $K_{\rm m}$ value was 67.62 μM, determined by varying the probe 2 concentration and fitting the fluorescence increase using the Michaelis-Menten equation (Fig. 1f) [34]. The results above suggest that 2 could be catalytically activated by caspase-3 with good sensitivity, enabling the monitoring of caspase-3 expression. The fluorescence increase could be clearly visualized using an IVIS optical imaging system (Fig. 1g).

The binding affinity of **2** to PSMA was evaluated by an NAALADase assay [30]. The K_i value was determined to be 4.12 nM (Fig. S4), indicating a strong affinity to the PSMA protein. A docking study of **2** with the X-ray crystal structure of PSMA (PDB ID: 5O5R) was performed (Fig. 1h). The α -and γ -carboxylic acid of the P1' glutamate in probe **2** formed strong interactions with Arg 210 and Lys 699, respectively, and the carboxylic group in the P1 site formed hydrogenbonding interactions with Arg 536, which is the key residue of the arginine patch region for strong PSMA-binding



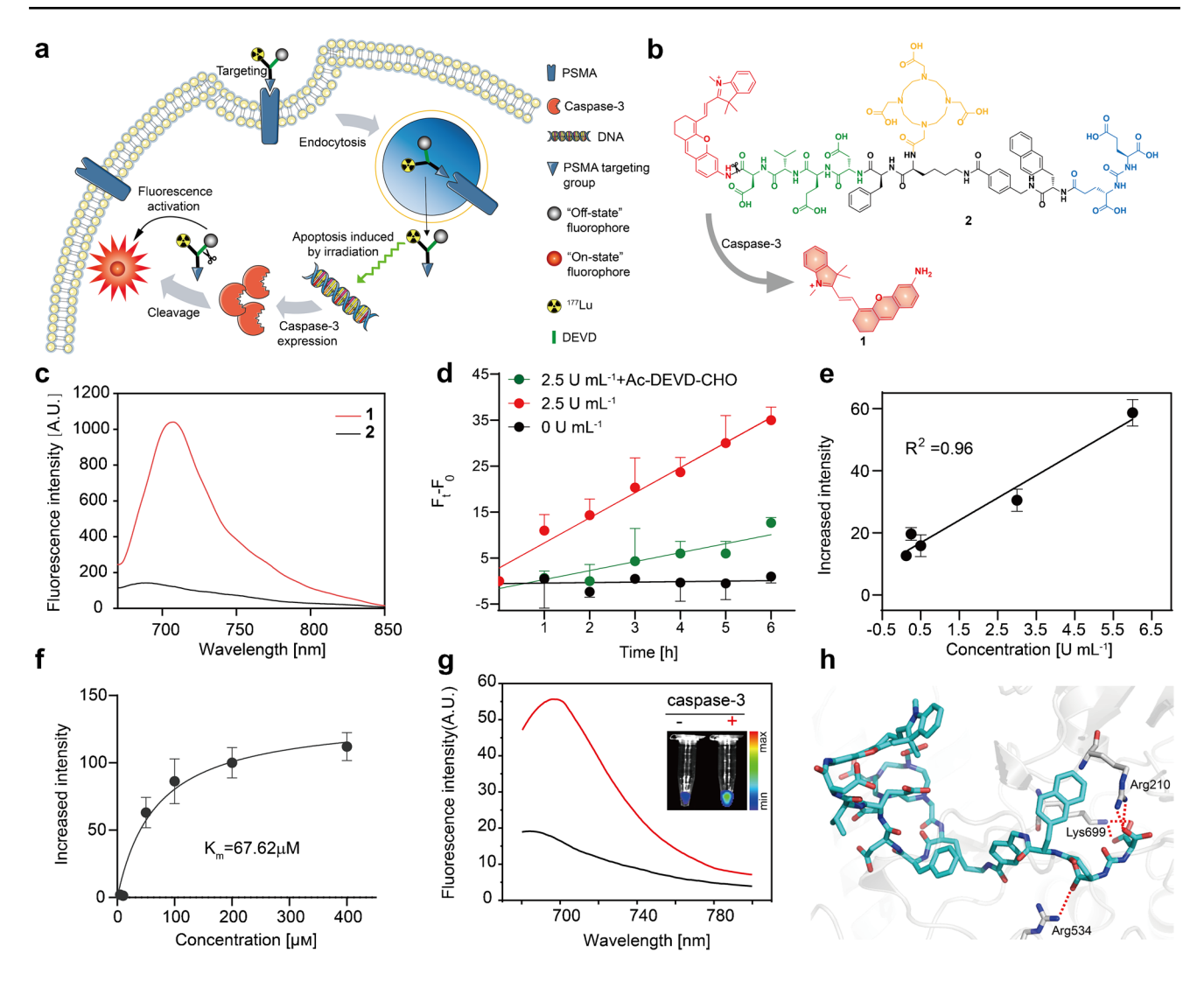


Fig. 1 Strategy, structure, and properties of the radiation activatable probe. a Schematic of the probe design. b The structure of the probes. c Fluorescence emission spectra of 1 and 2. 5 μ M and 670 nm excitation. d Time-dependent fluorescence change of 2 catalyzed by caspase-3. Ac-DEVD-CHO is a caspase-3 inhibitor. Ft-F₀ is the fluorescence enhancement. n=3. One "U" indicates the enzyme activity that cleaves 1 nmol of the caspase substrate DEVD-pNA (pNA: pnitro-

analine) per hour at 37 °C. **e** Caspase-3 concentration-dependent fluorescence change of 2. n=3. **f** Michaelis–Menten curve of 2. Five to 400 μ M of 2 were treated with 2.5 U/ml of caspase-3 at 37 °C for 6 h. n=3. **g** Fluorescence images of 2 responding to caspase-3. 10 μ M of 2 and 2.5 U/ml caspase-3 were incubated at 37 °C for 48 h. **h** Docking result of 2 in complex with PSMA protein. Data in panels **d**, **e**, and **f** are presented as mean values \pm SD

ligands. The caspase-3 activatable dye was located on the surface area of PSMA, making it accessible to caspase-3 to trigger signal release. After optimization, **2** could be conveniently radiolabeled with ¹⁷⁷Lu with > 98% radiochemical yield by heating the ligand with [¹⁷⁷Lu]-LuCl₃ in buffer at 85–90 °C for 10 min (Fig. S5).

Cellular study of the radiation-triggered probe-targeting PSMA

The cytotoxicity of **2** was measured using an MTT-based viability assay. LNCaP, 22Rv1, and PC3 cell lines expressing high, medium, and negligible levels of PSMA were

selected for cellular studies [35, 36]. No significant toxic effect was observed up to 200 μ M for any of the cell lines (Fig. 2a). ¹⁷⁷Lu-labeled **2** was applied to determine the PSMA-specific cellular uptake of the probe. The radioactivity uptake values for LNCaP and 22Rv1 cells were $1.11 \pm 0.08\%$ ID/10⁵ cells and $0.50 \pm 0.02\%$ ID/10⁵ cells, which were 6.2 and 2.8 times higher than those of PC3 cells (Fig. 2b). This uptake could be significantly blocked by a known PSMA inhibitor, ZJ43 [37]. The internalization ratios for LNCaP and 22Rv1 cells were 72% and 56%, respectively (Fig. 2c). To test the detection limit of this probe and mimic the heterogeneity expression of PSMA in patients, the 22Rv1 cell line was selected for subsequent



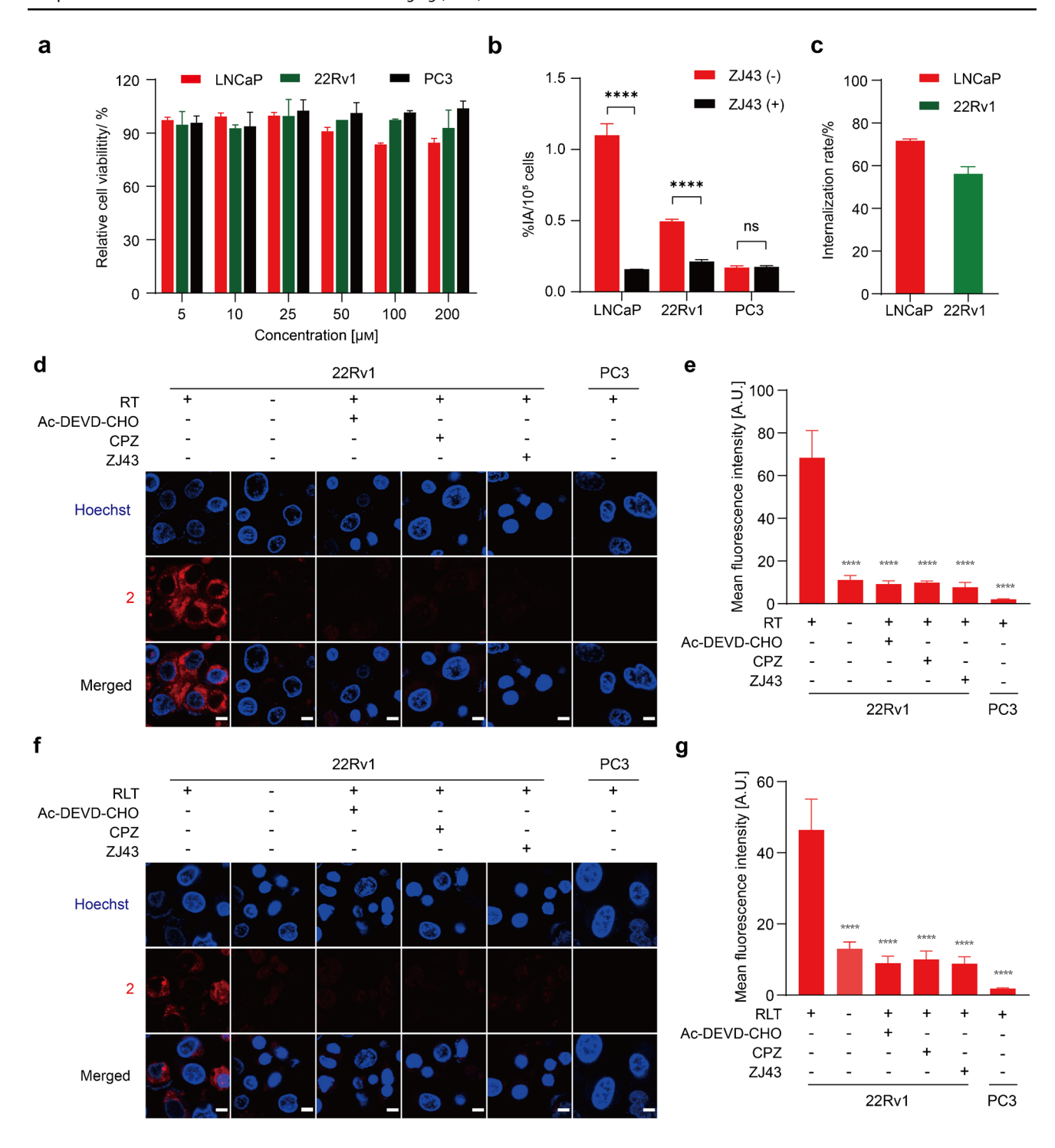


Fig. 2 The cellular study of the radiation activatable probe. **a** Cytotoxicity of 2 was determined by the MTT viability assay. n=3. **b** The radioactivity uptake of ¹⁷⁷Lu-labeled 2 in LNCaP, 22Rv1, and PC3 cells. PSMA inhibitor ZJ43 was applied in the control group. n=3. **c** The radioactivity internalization ratio of ¹⁷⁷Lu-labeled 2 in LNCaP and 22Rv1 cells. **d** Fluorescence images of PSMA-expressing cells incubated with 2 in response to external radiation. PSMA⁺ 22Rv1 cells were radiated at 8 Gy. Control groups were no radiation, pretreated with 50 μM caspase-3 inhibitor, pretreated with 10 μM endocytosis inhibitor (CPZ, Chlorpromazine), and pretreated with 100 μM PSMA inhibitor (ZJ43) and PSMA⁻ PC3 cells. Cell nuclei were stained with hochest 33,342 and shown in blue. The activated probe

was shown in red. Scale bar: $10 \ \mu m$. **e** Quantification of the fluorescence intensity of samples in panel **d**. n=5 randomly selected fields. **f** Fluorescence images of PSMA-expressing cells incubated with 2 in response to 177 Lu-RLT. PSMA+ 2 22Rv1 cells were treated with 370 kBq 177 Lu-labeled 2. The control groups were set similar to **d**. Cell nuclei were stained with hochest 33,342 and shown in blue. The activated probe was shown in red. Scale bar: $10 \ \mu m$. **g** Quantification of the fluorescence intensity of samples in panel **f**. n=5 randomly selected fields. Data in **a**, **b**, **c**, **e**, and **g** are presented as mean values \pm SD. Asterisk (****) indicates P values < 0.0001, ns indicates non-statistically significant. Two-tailed unpaired Student t-test for **b**, one-way ANOVA Tukey's multiple comparisons test for **e** and **g**



experiments, and the PC3 cell line was used as a negative control.

For the cell imaging study, we initially chose external X-ray radiation to induce apoptosis [11, 38], which makes it easy to control the radiation dose. Initially, we optimized the radiation doses and selected the lowest radiation dose that could produce a significant difference from the control group for the following experiments (Fig. S6). After irradiation with 8 Gy to induce caspase-3 expression [39], the cells were treated with 100 µM 2 for another 12 h and subsequently imaged with fluorescence confocal microscopy. A specific fluorescence signal could only be activated in PSMA⁺ 22Rv1 cells with radiation, in comparison to no radiation, caspase-3 inhibition, PSMA-mediated endocytosis inhibition, PSMA-binding inhibition, and PSMA-PC3 groups (Fig. 2d). Quantification of the signal showed that the fluorescence intensity of the radiation treatment group was 6.15 to 32.86 times higher than that of the control groups (Fig. 2e). The results suggest that the fluorescence activation of 2 requires PSMA-specific binding, effective endocytosis, and the expression of caspase-3, which makes the probe highly specific to radiation and PSMA expression.

Since the method was validated using external X-ray radiation, we next investigated the feasibility of imaging ¹⁷⁷Lu-PSMA-targeted RLT, where the radiation is mainly in β-particles and limited by the PSMA expression level. After the prostate cancer cells were treated with 370 kBq ¹⁷⁷Lu-labeled **2**, similar procedures were applied for fluorescence confocal microscopy. Only PSMA⁺ 22Rv1 cells showed fluorescence activation (Fig. 2f). The fluorescence intensity was 3.57 to 25.43 times higher than that of the control groups in a radiation- and PSMA-dependent manner (Fig. 2g). The results indicate that this method displays good sensitivity for detecting RLT-induced apoptosis even with low PSMA expression at the cellular level.

In vivo monitoring external radiation therapy

We then carried out in vivo imaging studies, and external radiation was first performed to validate the method. The 22Rv1 or PC3 tumor mice were treated with an 8 Gy dose of external X-ray radiation at the tumor sites, and then the mice were administered 200 nmol 2 via the tail vein at 48 h postradiation. Fluorescence imaging was performed at 1 h, 4 h, 12 h, 24 h, 48 h, and 72 h (Fig. 3a). The quantification of the signal intensity for 22Rv1 and PC3 tumors was summarized at different time points (Fig. 3b, c). PC3 tumors could not be visualized, and there was no significant difference in fluorescence intensity between the groups with or without radiation (Fig. 3a and c). These results indicate that without PSMA receptor binding and internalization, radiation-induced caspase-3 could not achieve effective signal activation. In contrast, 22Rv1 tumors could be visualized, showing the weak

signal from **2** upon binding to PSMA compared with PC3 tumors, and there was a maximum 1.72-fold fluorescence signal enhancement for the radiation-treated group, indicating the upregulation of caspase-3 (Fig. 3a, b). The signal increase could be clearly observed and preserved for all the time points tested.

At the end of the experiment, the mice were sacrificed, and the organs of interest were collected for ex vivo fluorescence quantification, which was in agreement with in vivo observations (Figs. 3d, e, S10). 22Rv1 tumors treated with radiation had the highest fluorescence signal resulting from the PSMA binding of 2 and caspase-3-triggered signal activation. The highest signal was found in the kidneys, and the liver also accumulated a higher signal than other organs, illustrating the pharmacokinetic character of this probe.

To validate caspase-3 expression, the resected tumor samples were stained with caspase-3 antibody and imaged under confocal microscopy (Fig. 3f, h, and Fig. S11a, c). Elevated caspase-3 expression was clearly observed in both 22Rv1 and PC3 tumors treated with radiation. The fluorescence activation of probe 2 was only detected in 22Rv1 tumors and showed colocalization with caspase-3 (Fig. 3g, i, and Fig. S11b, d). The results indicate that 2 can specifically detect PSMA and caspase-3 co-expression in vivo and can be used to image the external radiation treatment response of prostate cancer.

In vivo monitoring ¹⁷⁷Lu-RLT

After we validated the method for in vivo imaging of the external radiation treatment response, we then investigated the feasibility of imaging the more challenging ¹⁷⁷Lu-RLT. Before we attempted to image the treatment response of ¹⁷⁷Lu-labeled **2**, we first evaluated the in vivo distribution of the radioligand in 22Rv1 tumors. Mice bearing 22Rv1 tumors were injected with 18.5 MBq ¹⁷⁷Lu-labeled **2** and SPECT/CT imaging was performed at 24 h post-injection. 22Rv1 tumors could be clearly visualized, indicating specific radioactivity accumulation in PSMA-expressing tumors (Fig. 4a). To quantify the imaging results, we carried out an ex vivo biodistribution (Figs. 4b, c, S12). The tumor uptake was 1.06% ID/g, and the tumor-to-blood ratio and tumor-to-muscle ratio were 3.97 and 5.05, respectively, which were in agreement with SPECT imaging.

We then attempted to image the treatment response of ¹⁷⁷Lu-RLT using activatable fluorescence probe **2**. After 22Rv1 tumors were treated with or without 18.5 MBq ¹⁷⁷Lu-**2** for 48 h, 200 nmol **2** was administered via the tail vein. Fluorescence imaging was performed at 1 h, 4 h, 12 h, 24 h, 48 h, and 72 h (Fig. 4d). Specific signal activation could only be observed in ¹⁷⁷Lu-treated tumors. The quantification results showed a maximum 1.79-fold fluorescence enhancement between the treated and nontreated groups (Fig. 4e),



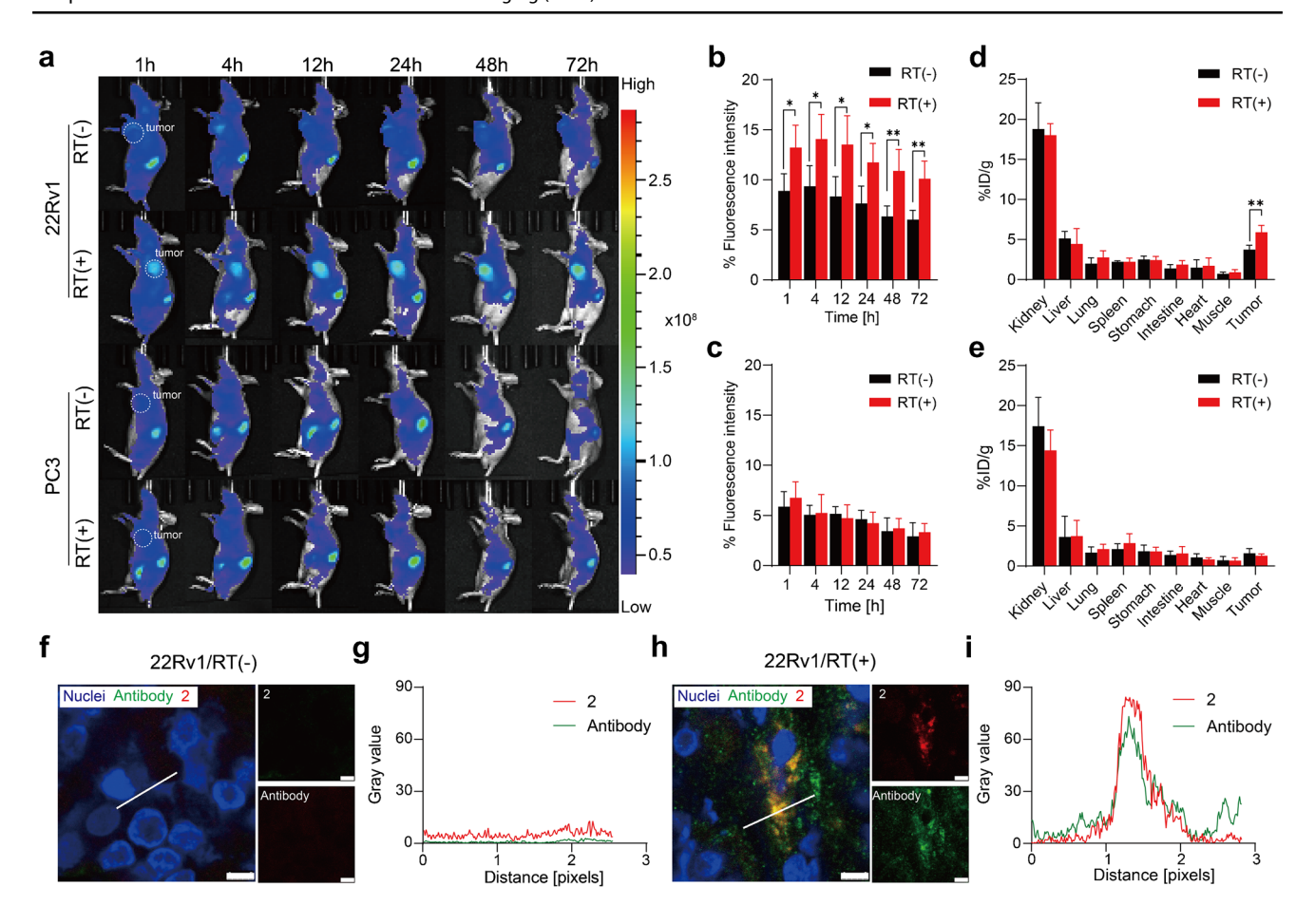


Fig. 3 In vivo monitoring the prostate tumor response to the RT treatment. a Fluorescence imaging of 22Rv1 and PC3 tumors. The tumors were pretreated with or without 8 Gy of radiation, and the mice were administrated with 200 nmol 2 via tail vein at 48 h post-radiation. The fluorescence images were acquired at 1 h, 4 h, 12 h, 24 h, and 72 h post-administration. The white dotted circle indicates the location of the tumor. **b–c** Quantitative analysis of fluorescence intensity of 22Rv1 and PC3 tumors in panel **a**. n=5 for radiation treatment groups and n=4 for no radiation groups. **d–e** Ex vivo quantitative analysis of fluorescence organ distribution of 22Rv1 and PC3 tumors at 72 h post-administration in panel **a**. **f** Fluorescence imaging of caspase-3 and activated probe in 22Rv1 tumor slices without radiation.

Caspase-3 was stained with antibodies and shown in green. Activated probes were shown in red. Scale bar: 10 μ m. **g** Correlation between antibody and activated probe. Fluorescence intensities corresponding to cross-section (white line) in panel **f**. **h** Fluorescence imaging of caspase-3 and activated probe in 22Rv1 tumor slices with radiation. Caspase-3 was stained with antibodies and shown in green. Activated probes were shown in red. Scale bar: 10 μ m. **i** Correlation between antibody and activated probe. Fluorescence intensities corresponding to cross-section (white line) in panel **h**. Data in panels **b**–**e** are presented as mean values \pm SD. (*) indicates P values < 0.05, (**) indicates P values < 0.01. Two-tailed unpaired Student t-test

which was also further confirmed by ex vivo fluorescence quantification (Fig. 4f). Under similar conditions, PC3 tumors were also tested as control groups, which showed no significant difference in fluorescence intensity between the treated and nontreated groups (Fig. S13a–d). The resected tumor samples were further stained with caspase-3 antibody and imaged under confocal microscopy (Fig. 4g, i, and Fig. S14a, c). Elevated caspase-3 expression was only clearly observed in 22Rv1 tumors treated with ¹⁷⁷Lu-RLT, which is consistent with the fluorescence signal of probe 2 activation (Fig. 4g–j and Fig. S14a–d). These results indicate that PSMA targeting ¹⁷⁷Lu-RLT upregulates caspase-3 and that the probe can be specifically turned on by PSMA- and caspase-3-expressing cells in vivo. In addition, we measured

the radiation toxicity of ¹⁷⁷Lu-**2** and found that it showed no obvious damage to the major organs (Fig. S15). Overall, we successfully demonstrate that PSMA-targeting probe **2** can specifically image the radiation treatment response of RLT in prostate tumors.

Discussion

PSMA, which is overexpressed in almost all prostate cancers and shows limited expression in normal tissues, has been proven to be a valuable biomarker for the diagnosis and treatment of prostate cancer. Low-molecular-weight PSMA targeting agents have been successfully applied to



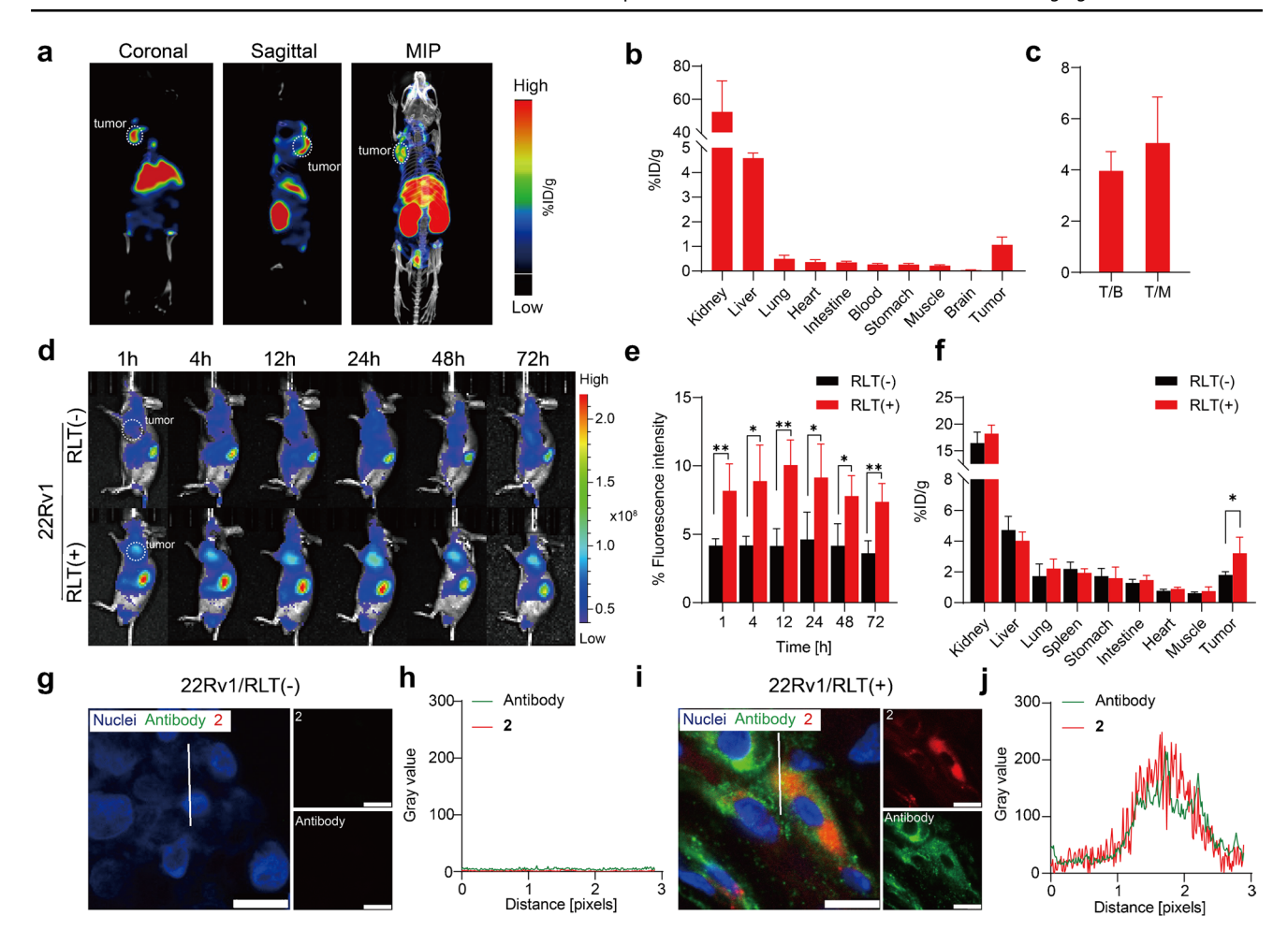


Fig. 4 In vivo monitoring the prostate tumor response to the ¹⁷⁷Lu-RLT treatment. **a** The SPECT/CT imaging of 22Rv1 tumors. Mice were injected with 18.5 MBq ¹⁷⁷Lu-labeled 2 via tail vein, the images were acquired at 24 h post-injection. The white dotted circle indicates the location of the tumor. **b** Biodistribution of ¹⁷⁷Lu-labeled 2 in 22Rv1 tumor-bearing mice at 24 h post-injection. n=4. **c** Tumor-to-blood (T/B) ratio and tumor-to-muscle (T/M) ratio in panel **b**. **d** Fluorescence imaging of 22Rv1 tumors treated with ¹⁷⁷Lu-RLT. Mice were injected with 18.5 MBq ¹⁷⁷Lu-labeled 2 or an equivalent amount of non-labeled 2, and 48 h later 200 nmol 2 was administrated via tail vein. The images were acquired at 1 h, 4 h, 12 h, 24 h, and 72 h post-administration. The dotted circle indicates the location of the tumor. **e** Quantification of fluorescence intensity of 22Rv1 tumors in panel **d**. n=4. **f** Ex vivo fluorescence intensity quantifica-

specifically deliver radioisotopes for translational research. Recently, the FDA approved ⁶⁸ Ga-PSMA-11 and ¹⁸F-DCF-PyL for PET imaging of prostate cancer, with improved sensitivity of 74–96% and specificity close to 100% [40–42]. β-emitter ¹⁷⁷Lu or α-emitter ²²⁵Ac-based RLT also showed promise for treating mCRPC with low toxic side effects and a high response rate in patients [4–6, 43]. Compared with conventional ways of evaluating treatment responses, an imaging-based method reflecting the early tumor response to RLT would provide timely information to assess radiation sensitivity and heterogeneity and therefore enhance

tion of the organs of 22Rv1 tumor-bearing mice at 72 h post-injection in panel **d**. n=4. **g** Fluorescence imaging of caspase-3 and activated probe in non-RLT treated 22Rv1 tumor slices. Caspase-3 was stained with antibodies and shown in green. Activated probes were shown in red. Scale bar: 10 µm. **h** Correlation between antibody and activated probe. Fluorescence intensities corresponding to cross-section (white lines) in panel **g**. **i** Fluorescence imaging of caspase-3 and activated probe in RLT treated 22Rv1 tumor slices. Caspase-3 was stained with antibodies and shown in green. Activated probes were shown in red. Scale bar: 10 µm. **j** Correlation between antibody and activated probe. Fluorescence intensities corresponding to cross-section (white lines) in panel **i**. Data in panels **b**, **c**, **e**, and **f** are presented as mean values \pm SD. (*) indicates P values < 0.05, (**) indicates P values < 0.01. Two-tailed unpaired Student t-test

RLT-based personalized therapy. With this aim, we initiated this pilot study and designed a PSMA-targeting RLT agent conjugated with a caspase-3-activatable fluorescence switch as a self-triggered probe for sensing apoptosis events.

Probe **2** can potently bind to PSMA with a K_i of 4.12 nM, consistent with our docking study. The fluorescence signal can be catalytically switched on by caspase-3 with a K_m of 67.62 μ M and a detection limit approaching 0.125 U/ml. A cellular study proved that **2** could specifically image PSMA⁺ cells treated with either external X-ray or β -emitter ¹⁷⁷Lu-RLT. PSMA binding, receptor-mediated endocytosis, and



upregulation of caspase-3 are responsible for the high specificity. In contrast to external radiation, the effective dose of RLT is mainly limited by the receptor density expressed on the targeted cells. The probe was tested in a medium PSMA-expressing 22Rv1 tumor model to mimic the extreme case of RLT. The imaging of the treatment response showed a 1.79-fold increase in fluorescence, which is similar to the results of a 1.72-fold increase observed for external radiation. The combined effects of site-specific radiation of RLT and the relatively high local concentration of the β -emitter within the tumor may be responsible for magnifying the signal. We successfully demonstrate for the first time that it is feasible to image the biological responses to RLT by activatable fluorescence probes, which may provide insight into the design of RLT activatable sensors or prodrugs in general.

Conclusion

In summary, we developed an activatable fluorescence probe specifically targeting PSMA and caspase-3 coexpression to monitor early treatment responses to RLT. Probe 2 can potently bind to PSMA, and the fluorescence signal can be switched on by caspase-3 with sensitivity. Cellular and in vivo studies prove that signal activation depends on both radiation-stimulated caspase-3 upregulation and PSMA-mediated endocytosis, enabling its high selectivity. Using a medium PSMA-expressing xenograft model, we demonstrated that 2 could achieve 1.79 times signal activation upon treatment with ¹⁷⁷Lu-RLT, which may provide a tool to investigate and optimize RLT.

Supplementary Information The online version contains supplementary material available at https://doi.org/10.1007/s00259-022-05743-7.

Author contribution Xing Yang and Zhaofei Liu conceived and designed research. Hongchuang Xu performed the chemical synthesis. Hongchuang Xu and Xuekang Cai measured the absorption and emission spectrum. Jingming Zhang performed in vitro caspase-3 protein assay and PSMA inhibition experiments. Hyunsoo Ha and Youngjoo Byun performed the docking study. Xiaojiang Duan and Yanpu Wang performed radiolabeling experiments. Xiaojiang Duan performed cell uptake experiments. Yanpu Wang and Ting Zhang designed and performed live cell imaging experiments and SPECT/ CT imaging experiments. Yanpu Wang performed the mouse imaging. Hongchuang Xu, Yanpu Wang, Jingming Zhang, Xing Yang, and Zhaofei Liu analyzed data. Xing Yang, Zhaofei Liu, Jingming Zhang, Hongchuang Xu, Yanpu Wang, and Xuekang Cai wrote the original draft. Xing Yang, Zhaofei Liu, Yanpu Wang, Yan Fan, and Zhi Yang reviewed and edited the draft. All authors discussed the results and commented on the manuscript.

Funding This work was financially supported by the National Natural Science Foundation of China (92059101, 21877004, 81873907, and 81920108020), National Key R&D Program of China (2018YFE0205300 and 2018YFC1313300), Beijing Natural Science Foundation (JQ19026), Clinical Medicine Plus X-Young Scholars

Project of Peking University (PKU2020LCXQ029), and the Fundamental Research Funds for the Central Universities (BMU2021RCZX018 and PKU2019LCXQ023). This work was in part supported by the National Research Foundation of Korea (2019R1A6A1A03013807 and 2020R1A2C2005919).

Availability of data and material Not applicable.

Code availability Not applicable.

Declarations

Ethics approval All animal studies were carried out in conformity to regulations on laboratory animals of the Beijing municipality and approved by the Animal Ethics Committee at Peking University Frist Hospital (Beijing, China), approval number J202163.

Consent to participate Not applicable.

Consent for publication Not applicable.

Conflict of interest The authors declare no competing interests.

Clinical trial registration Not applicable.

References

- Sung H, Ferlay J, Siegel RL, et al. Global cancer statistics 2020: global estimates of incidence and mortality worldwide for 36 cancers in 185 countries. CA Cancer J Clin. 2021;71:209–49.
- Litwin MS, Tan HJ. The diagnosis and treatment of prostate cancer: a review. JAMA J Am Med Assoc. 2017;317:2532–42.
- Rebello RJ, Oing C, Knudsen KE, et al. Prostate cancer. Nat Rev Dis Primers. 2021;7:9.
- Hofman MS, Violet J, Hicks RJ, et al. [177 Lu]-PSMA-617 radionuclide treatment in patients with metastatic castration-resistant prostate cancer (LuPSMA trial): a single-centre, single-arm, phase 2 study. Lancet Oncol. 2018;19:825–33.
- Sartor O, de Bono J, Chi KN, et al. Lutetium-177–PSMA-617 for metastatic castration-resistant prostate cancer. N Engl J Med. 2021;385:1091–103.
- Hofman MS, Emmett L, Sandhu S, et al. [177Lu]Lu-PSMA-617 versus cabazitaxel in patients with metastatic castration-resistant prostate cancer (TheraP): a randomised, open-label, phase 2 trial. Lancet. 2021;397:797–804.
- Langbein T, Weber WA, Eiber M. Future of theranostics: an outlook on precision oncology in nuclear medicine. J Nucl Med. 2019;60:13S-S19.
- Wüstemann T, Haberkorn U, Babich J, Mier W. Targeting prostate cancer: prostate-specific membrane antigen based diagnosis and therapy. Med Res Rev. 2019;39:40–69.
- Fendler WP, Rahbar K, Herrmann K, Kratochwil C, Eiber M. ¹⁷⁷Lu-PSMA radioligand therapy for prostate cancer. J Nucl Med. 2017;58:1196–200.
- Gafita A, Heck MM, Rauscher I, et al. Early prostate-specific antigen changes and clinical outcome after ¹⁷⁷Lu-PSMA radionuclide treatment in patients with metastatic castration-resistant prostate cancer. J Nucl Med. 2020;61:1476–83.
- 11 Lee BS, Cho YW, Kim GC, et al. Induced phenotype targeted therapy: radiation-induced apoptosis-targeted chemotherapy. J Natl Cancer Inst. 2015;107:dju403.



- Fu Q, Li H, Duan D, et al. External-radiation-induced local hydroxylation enables remote release of functional molecules in tumors. Angew Chemie Int Ed Engl. 2020;59:21546–52.
- 13. Geng J, Zhang Y, Gao Q, et al. Switching on prodrugs using radiotherapy. Nat Chem. 2021;13:805–10.
- Paschalis A, Sheehan B, Riisnaes R, et al. Prostate-specific membrane antigen heterogeneity and DNA repair defects in prostate cancer. Eur Urol. 2019;76:469–78.
- Zhang J, Chai X, He XP, Kim HJ, Yoon J, Tian H. Fluorogenic probes for disease-relevant enzymes. Chem Soc Rev. 2019;48:683–722.
- Porter AG, Jänicke RU. Emerging roles of caspase-3 in apoptosis. Cell Death Differ. 1999;6:99–104.
- Huang Q, Li F, Liu X, et al. Caspase 3-mediated stimulation of tumor cell repopulation during cancer radiotherapy. Nat Med. 2011;17:860-6.
- Edgington LE, Berger AB, Blum G, et al. Noninvasive optical imaging of apoptosis by caspase-targeted activity-based probes. Nat Med. 2009;15:967–73.
- He X, Hu Y, Shi W, Li X, Ma H. Design, synthesis and application of a near-infrared fluorescent probe for in vivo imaging of aminopeptidase N. Chem Commun. 2017;53:9438–41.
- Yuan Y, Kwok RTK, Tang BZ, Liu B. Targeted theranostic platinum(IV) prodrug with a built-in aggregation-induced emission light-up apoptosis sensor for noninvasive early evaluation of its therapeutic responses in situ. J Am Chem Soc. 2014;136:2546–54.
- Zeng Z, Liew SS, Wei X, Pu K. Hemicyanine-based near-infrared activatable probes for imaging and diagnosis of diseases. Angew Chemie Int Ed Engl. 2021;60:2–24.
- Yuan L, Lin W, Yang Y, Chen H. A unique class of near-infrared functional fluorescent dyes with carboxylic-acid-modulated fluorescence on/off switching: rational design, synthesis, optical properties, theoretical calculations, and applications for fluorescence imaging in living animals. J Am Chem Soc. 2012;134:1200–11.
- Cheng D, Peng J, Lv Y, et al. *De novo* design of chemical stability near-infrared molecular probes for high-fidelity hepatotoxicity evaluation *in vivo*. J Am Chem Soc. 2019;141:6352–61.
- Cheng P, Miao Q, Li J, Huang J, Xie C, Pu K. Unimolecular chemo-fluoro-luminescent reporter for crosstalk-free duplex imaging of hepatotoxicity. J Am Chem Soc. 2019;141:10581–4.
- He X, Li L, Fang Y, Shi W, Li X, Ma H. *In vivo* imaging of leucine aminopeptidase activity in drug-induced liver injury and liver cancer via a near-infrared fluorescent probe. Chem Sci. 2017;8:3479–83.
- Tian X, Li Z, Ding N, Zhang J. Near-infrared ratiometric selfassembled theranostic nanoprobe: imaging and tracking cancer chemotherapy. Chem Commun. 2020;56:3629–32.
- Rhéaume E, Cohen LY, Uhlmann F, et al. The large subunit of replication factor C is a substrate for caspase-3 in vitro and is cleaved by a caspase-3-like protease during fas-mediated apoptosis. EMBO J. 1997;16:6346–54.
- Kozikowski AP, Nan F, Conti P, et al. Design of remarkably simple, yet potent urea-based inhibitors of glutamate carboxypeptidase II (NAALADase). J Med Chem. 2001;44:298–301.
- Yang X, Mease RC, Pullambhatla M, et al. Fluorobenzoyllysinepentanedioic acid carbamates: new scaffolds for positron emission

- tomography (PET) imaging of prostate-specific membrane antigen (PSMA). J Med Chem. 2016;59:206–18.
- 30. Duan X, Liu F, Kwon H, et al. (S)-3-(Carboxyformamido)-2-(3-(carboxymethyl)ureido)propanoic acid as a novel PSMA targeting scaffold for prostate cancer imaging. J Med Chem. 2020;63:3563–76.
- 31. Müller C, Van Der Meulen NP, Benešová M, Schibli R. Therapeutic radiometals beyond 177Lu and 90Y: production and application of promising α-particle, β–particle, and auger electron emitters. J Nucl Med. 2017;58:91S-S96.
- Benesová M, Schäfer M, Bauder-Wüst U, et al. Preclinical evaluation of a tailor-made DOTA-conjugated PSMA inhibitor with optimized linker moiety for imaging and endoradiotherapy of prostate cancer. J Nucl Med. 2015;56:914–20.
- Garcia-Calvo M, Peterson EP, Leiting B, Ruel R, Nicholson DW, Thornberry NA. Inhibition of human caspases by peptide-based and macromolecular inhibitors. J Biol Chem. 1998;273:32608–13.
- Choi B, Rempala GA, Kim JK. Beyond the Michaelis-Menten equation: accurate and efficient estimation of enzyme kinetic parameters. Sci Rep. 2017;7:17018.
- 35 Chang Lee S, Ma JSY, Kim MS, et al. A PSMA-targeted bispecific antibody for prostate cancer driven by a small-molecule targeting ligand. Sci Adv. 2021;7:eabi8193.
- Kiess AP, Minn I, Chen Y, et al. Auger radiopharmaceutical therapy targeting prostate-specific membrane antigen. J Nucl Med. 2015;56:1401–7.
- Olszewski RT, Bukhari N, Zhou J, et al. NAAG peptidase inhibition reduces locomotor activity and some stereotypes in the PCP model of schizophrenia via group II mGluR. J Neurochem. 2004:89:876–85.
- Cho YW, Kim SY, Kwon IC, Kim IS. Complex adaptive therapeutic strategy (CATS) for cancer. J Control Release. 2014;175:43–7.
- Zhao Y, Zhang T, Wang YP, et al. ICAM-1 orchestrates the abscopal effect of tumor radiotherapy. Proc Natl Acad Sci USA. 2021;118:e2010333118.
- Hofman MS, Lawrentschuk N, Francis RJ, et al. Prostatespecific membrane antigen PET-CT in patients with high-risk prostate cancer before curative-intent surgery or radiotherapy (proPSMA): a prospective, randomised, multicentre study. Lancet. 2020;395:1208–16.
- Eder M, Schäfer M, Bauder-Wüst U, et al. ⁶⁸Ga-complex lipophilicity and the targeting property of a urea-based PSMA inhibitor for PET imaging. Bioconjug Chem. 2012;23:688–97.
- Chen Y, Pullambhatla M, Foss CA, et al. 2-(3-{1-carboxy-5-[(6-[18F]fluoro-pyridine-3-carbonyl)-amino]- pentyl}-ureido)-pentanedioic acid, [18F]DCFPyL, a PSMA-based PET imaging agent for prostate cancer. Clin Cancer Res. 2011;17:7645–53.
- Zacherl MJ, Gildehaus FJ, Mittlmeier L, et al. First clinical results for PSMA-targeted α-therapy using ²²⁵Ac-PSMA-I&T in advanced-mCRPC patients. J Nucl Med. 2021;62:669–74.

Publisher's note Springer Nature remains neutral with regard to jurisdictional claims in published maps and institutional affiliations.

